EFFECT OF CURING STRESSES ON THE INTER-FIBRE FAILURE UNDER TRANSVERSE COMPRESSION

Elena Correa, Federico París and Vladislav Mantič

Group of Elasticity and Strength of Materials, School of Engineering, University of Seville
Camino de los Descubrimientos S/N, 41092 Sevilla, Spain
correa@esi.us.es

ABSTRACT

In the present work the influence at micromechanical scale of residual stresses appearing in the last stage of the manufacture of fibrous composite materials, i.e. the curing process, on the inter-fibre failure under transverse compression is studied. In particular, the effect of the presence of residual curing stresses on the appearance of the first debonds is discussed analytically, whereas later steps of the damage mechanism, i.e. the growth of interface cracks and their kinking towards the matrix, are analysed by means of a single fibre model, making use of the Boundary Element Method. The results are evaluated applying Interfacial Fracture Mechanics concepts. The conclusions obtained show that the effect of residual curing stresses on the appearance and initiation of growth to be negligible, and the morphology of the damage not to be significantly affected in comparison with the case in which these stresses are not considered.

1. INTRODUCTION

There exists a final stage in the manufacturing process of fibrous composites materials in which the curing of the material takes place. The differences in free contraction between the fibres and the matrix cause, during this stage of the process, the appearance of residual stresses. The presence of these stresses may affect both the strength and the stiffness of the laminate and also have influence on the development of failure mechanisms in the material.

The study of residual stresses at macro- and mesomechanical level is widely developed, there being several methods able to quantify them [1]. By contrast, at micromechanical level, due to the high complexity of the material at this scale, the measurement and prediction of residual stresses presents more difficulties. If knowledge of the mechanisms of failure at micromechanical level is considered to be fundamental for the development of failure criteria able to perform a more complete diagnosis of the appearance of these mechanisms [2], the analysis of the influence of curing stresses at this scale then acquires high relevance.

The particular case of the inter-fibre failure (also known as matrix failure) under transverse tension has already been the object of several micromechanical studies by the authors [3,4,5] and, more recently, the case of the inter-fibre failure under compression has also been undertaken [6,7]. These studies have made it possible to understand the initiation of failure at the micromechanical scale as well as its later progress, which leads to the macro-failure of the material. The inter-fibre failure under compression, typically appearing in impact problems and caused by a dominant compression acting transversely to the fibres, starts with the appearance of small debonds at the fibre-matrix interfaces. The initial defects present a non-symmetric morphology: a small ‘bubble’ at the lower crack tip and a contact zone at the upper crack tip, see Figure 2a, and, in a first period, grow unstably along the interfaces (interface cracks) following the lower crack tip. This period ends when these cracks have reached a certain length at the interface. From that moment on the growth of the

interface crack becomes stable, which favours the occurrence of a different stage of the mechanism of failure: the propagation of the crack through the matrix. Thus, the interface crack suddenly changes its direction of propagation, kinking into the matrix following an orientation angle around 53º from the direction perpendicular to the load. These numerical predictions agree with the experimental results obtained from broken specimens, Figure 1.

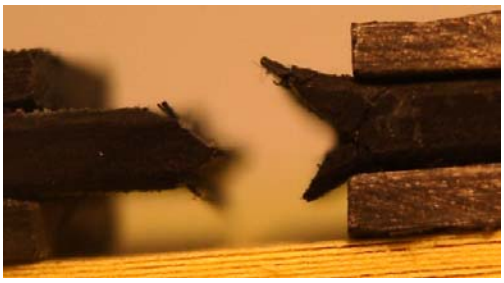

Figure.1. Matrix/Inter-fibre failure in carbon fibre specimens tested under transverse compression.

The present work is a continuation of the previous studies related to inter-fibre failure under transverse compression and analyses the influence of residual stresses, originated by the curing process, on the conclusions obtained so far and summed up in the previous paragraph. To this end a Boundary Elements single fibre model has been carried out and its results analysed using the concepts derived from Interfacial Fracture Mechanics.

2. SINGLE FIBRE MODEL

The study has been carried out using a tool based on the BEM [8], that makes it possible to perform the numerical analysis of plane elastic problems considering contact and interface cracks. Two BEM models are used in this analysis. The basic model employed is shown in Figure 2a and represents the case of a crack that, under the plain strain hypothesis, grows along the interface.

In order to characterize the problem from the Fracture Mechanics point of view the energy release rate, G, will be used. The expression employed, based on the virtual closure crack technique [9] for a circular crack that propagates from a certain debonding angle, α, Figure 2a, to $\alpha+\Delta\alpha$ ($\Delta\alpha$ being much smaller than the crack length), is:

$$G(\alpha,\Delta\alpha)=\frac{1}{2\Delta\alpha}\int_0^{\Delta\alpha}\{\sigma_{rr}(\alpha+\theta)\Delta u_r(\alpha-\Delta\alpha+\theta)+\sigma_{r\theta}(\alpha+\theta)\Delta u_\theta(\alpha-\Delta\alpha+\theta)\}d\theta \quad (1)$$

where σ_{rr} and $\sigma_{r\theta}$ represent, respectively, radial and shear stresses along the interface, and Δu_r and Δu_θ the relative displacements of the crack faces. θ is the circumferential coordinate with reference to axis 2. Both modes of fracture, I (associated to σ_{rr}) and II (associated to $\sigma_{r\theta}$), are obviously considered in Equation (1).

When the presence of an incipient crack in the matrix is considered, the previous model is altered to represent the case of a crack that has first grown along the interface and, once kinked into the matrix, is progressing through it, Figure 2b. In this case Equation (1) is appropriately adapted to a crack in a homogeneous material. The materials chosen for the analysis correspond to a typical configuration among fibre reinforced materials: a glass fibre-epoxy matrix system whose thermoelastic properties are listed in Table 1. The fibre radius considered has been $a=7.5\cdot10^{-6}\,m$.

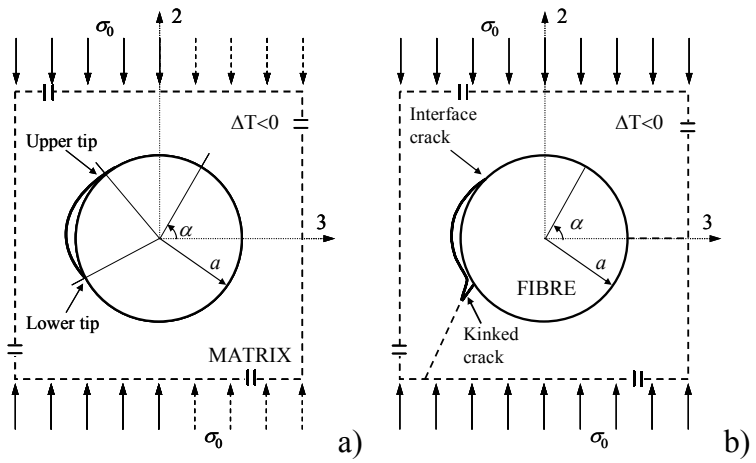

Figure 2: Single fibre model with a) interface crack, b) kinked crack

Dimensionless results for G will be presented in all cases. These dimensionless values are obtained, following [10, 11], by dividing the values of G by $G_0 = \left(\frac{1+\kappa^m}{8\mu^m}\right)\sigma_0^2 a\pi$, where $\kappa^m = 3-4\nu^m$, μ^m is the shear modulus of the matrix and σ_0 denotes the value of the applied compression.

Finally, the curing process employed in the case of the matrix considered in this work (epoxy resin) commonly consists of a first stage at environmental temperature followed by one or more stages at higher temperature. Independently of the temperature at which the curing process takes place, the contraction of the matrix (always higher than that of the fibre) leads the generation of residual stresses. This fact allows the inclusion of residual stresses in the analysis to be modelled by means of an adequate temperature decrease that captures the real curing contraction of the material. In the present work a matrix curing contraction of 0.4% has been considered, corresponding to a temperature decrease of 80 K.

Material	Poisson coefficient, ν	Young modulus, E	Coefficient of thermal expansion, α
Matrix (epoxy)	$\nu^m = 0.33$	$E^m = 2.79\times10^9\,\text{Pa}$	$\alpha^m = 52\times10^{-6}\,\text{K}^{-1}$
Fibre (glass)	$\nu^f = 0.22$	$E^f = 7.08\times10^{10}\,\text{Pa}$	$\alpha^m = 7\times10^{-6}\,\text{K}^{-1}$

Table 1: Thermoelastic properties of the materials.

Though the experimental evidence, Figure 1, corresponds to a carbon fibre composite the comparison with the numerical results is possible due to the weak dependence of the phenomenon under study of the properties of the materials [7].

3. ORIGIN OF DAMAGE

The beginning of the inter-fibre failure under transverse compression is considered to be controlled by the shear stress that acts at the fibre-matrix interface, under the hypothesis (not always corresponding exactly to reality) of an initially undamaged material. If the external compression is the only load considered it can be checked [6] that the zones of maximum shear stress, and therefore susceptible of housing the first debonds, are located at $\alpha = \pm 45^\circ, \pm 135^\circ$. Thus, the analysis of the effect of residual stresses on the initiation of failure must be carried out under the same premise, studying

the distribution of stresses around the interface when the fibre-matrix system suffers a thermal decrease corresponding to the curing contraction of the matrix. The consideration of real curing parameters, Section 2, unavoidably leads to the choice of external loads corresponding to real failure parameters. In particular, based on [12], the compressive strength of the unidirectional laminate chosen for the bimaterial system considered has been $Y_c = 115 \times 10^6$ Pa.

In this situation, an analysis of the stress state in a single fibre-configuration, assuming the interface to be initially in perfect condition and considering a temperature decrease of 80 K as a single solicitation, would allow the order of the curing stresses already existing to be estimated and their effect on the initiation of damage to be predicted. The problem presented in these terms can be solved analytically (plane problem of a fibre embedded in an infinite matrix) and the solution obtained shows that residual tractions are only produced in the radial direction, σ_{rr}. Thus, the consideration of curing residual stresses alters neither the location nor the critical load of the initial damage, since the curing process modelled in this study does not generate shear stresses.

4. THE INTERFACE CRACK

Although the consideration of residual curing stresses seems not to affect the initiation of failure it is necessary to analyse the influence of residual stresses over the growth of the first debonds. To this end the model appearing in Figure 2a is used in this section to carry out, by means of the BEM, an analysis of the interface crack growth under the combined action of an external compressive load (of value $\sigma_0 = 115 \times 10^6$ Pa) and a thermal decrease of 80 K. An initial 10º debond centred at $\alpha = 135$º (where the maximum shear stress is located) is supposed.

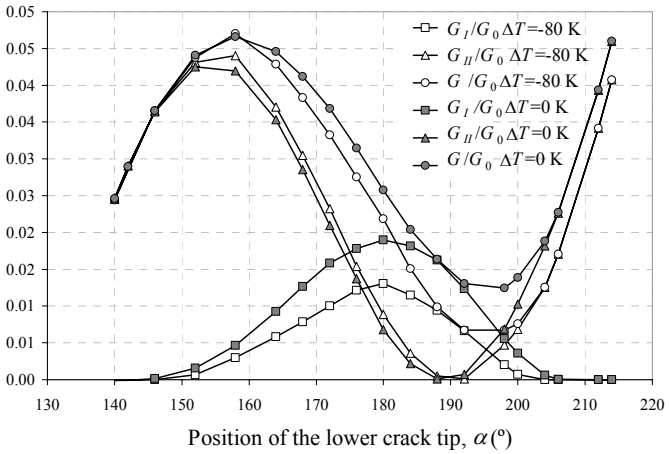

Figure 3. G evolution versus α ($\Delta T = 0\ K$ and $\Delta T = $ -80 K cases).

The results obtained, in terms of G versus the position of the lower crack tip, α, are presented in Figure 3 for the case under study ($\Delta T = $ -80 K in the Figure), which considers both residual curing stresses and the external compressive load, and for the case of single action of the external compressive load ($\Delta T = 0\ K$ in the Figure), used as a reference in this analysis and basis for the conclusions presented in [6,7]. It can be observed in the Figure how the consideration of residual curing stresses has no effect on the starting of the debond growth, since both evolutions coincide until an extension of the interface crack of about 20º is achieved. For later stages, yet, the G level is lower in the $\Delta T = $ -80 K case than in the $\Delta T = 0$ K case. This difference is mainly due

to the lower level reached by G_I in the ΔT = -80 K case, undoubtedly associated to the radial compressions present as a consequence of the curing process. The difference between G_{II} values of both cases is insignificant.

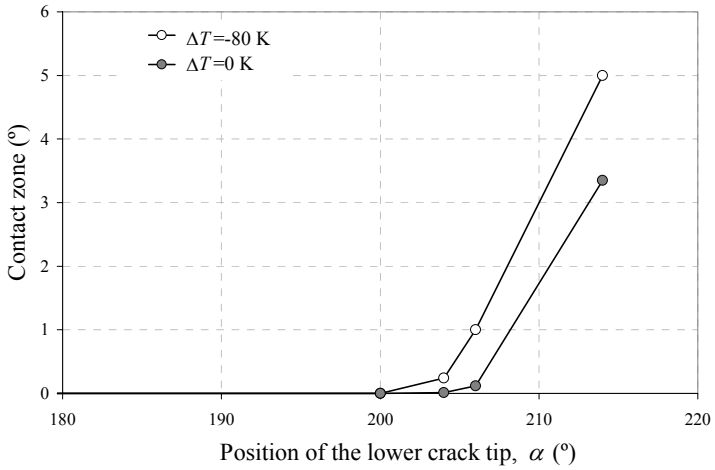

Figure 4. Contact zone evolution ($\Delta T = 0\ K$ and $\Delta T = -80\ K$ cases).

A similar morphology is found for the ΔT = -80 K interface crack and for the $\Delta T = 0$ K one, but, looking at Mode I evolution in more detail, Figure 3, it can be detected that the disappearance of this mode, associated to the closing of the existing 'bubble' at the lower crack tip and subsequent development of the physically relevant contact zone, slightly advances with reference to the original case, $\Delta T = 0$ K. This fact can be deduced from Figure 4, where the contact zone developed at the lower crack tip is represented versus its position at the interface. Numerical results show that the contact zone appears for a slightly lower crack size in the ΔT = -80 K case than in the $\Delta T = 0$ K case (approximately 202º versus 205º) and its extension is always greater in the ΔT = -80 K case.

In order to be able to perform predictions about the growth of the interface crack it is necessary, [13], to have an estimation of the critical value of G, G_c, which depends on the evolution of the fracture mixity, given by the local phase angle of the Stress Intensity Factor, ψ_K, and therefore function of α. The evolution considered in this work for G_c is based on the empirical and simplified proposal by Hutchinson and Suo [14]:

$$G_c(\psi_K) = G_{1c}\left(1 + \tan^2(1-\lambda)\psi_K\right), \tag{2}$$

where G_{1c} is the critical value of G_c for Mode I and λ is the fracture mode sensitivity parameter. Local phase angle ψ_K has been calculated following [15]:

$$\psi_K = 0.5 \arccos\left[F(\varepsilon)^{-1}\frac{G_I - G_{II}}{G_I + G_{II}}\right], \tag{3}$$

where $F(\varepsilon) = 1 + \left(\pi^2/3 - 2\right)\varepsilon^2 + O\left(\varepsilon^4\right)$, ε being the oscillatory index which, for the bimaterial system employed, takes the value $\varepsilon = -0.074$.

This approach was already employed in [6] to predict the growth of the interface crack for the $\Delta T = 0\ K$ case, making use of three different values of λ (within the range of

typical values): $\lambda = 0.2$, $\lambda = 0.25$ and $\lambda = 0.3$. In that case, due to the absence of direct experimental data, the value of G_{1c} chosen for each λ was forced to fulfil the expression $G = G_c(\psi_K)$ for $\alpha = 140º$. The results provided by the comparison between the values of G and G_c calculated in this manner, predicted an unstable growth of the interface crack up to a lower crack tip position $\alpha \cong 206º$.

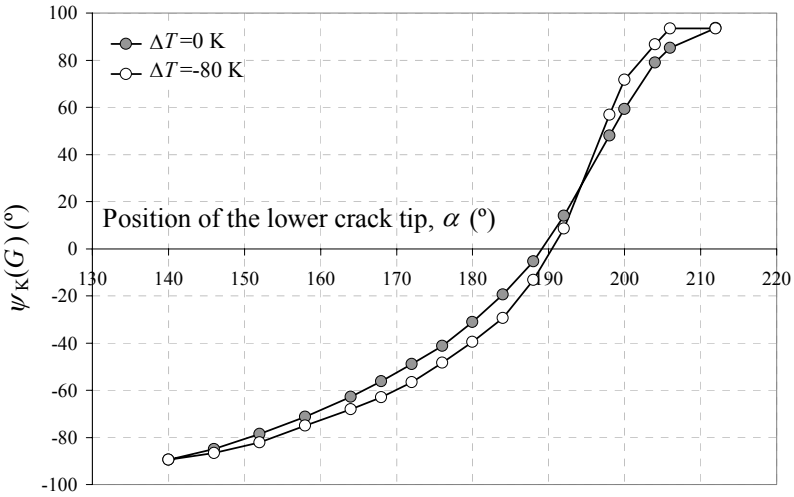

Figure 5. $\psi_K(G)$ versus α for the cases ΔT = -80 K and $\Delta T = 0$ K.

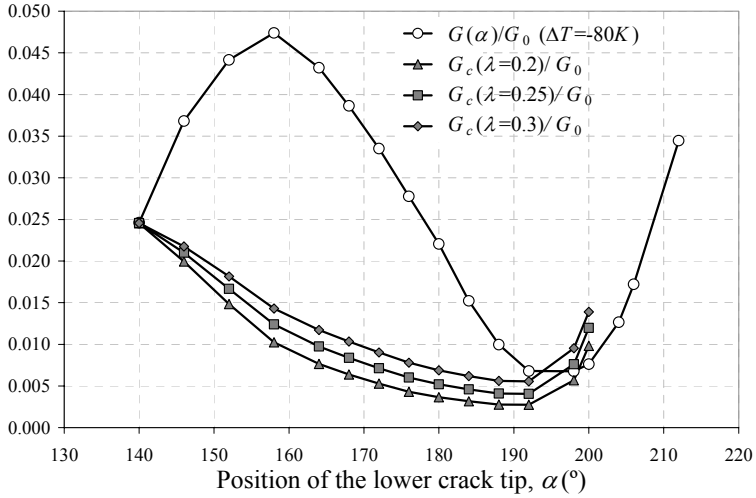

Figure 6. Comparison between G and G_c of the interface crack (ΔT = -80 K case).

The same process has been implemented in the present work for the case that includes the presence of the residual stresses, ΔT = -80 K. First of all, the evolution of $\psi_K(G)$, calculated from Equation (3), is presented in Figure 5. The small differences between both curves can be appreciated in this Figure as well as the earlier arrival of $\psi_K(G)$ to the 90º limit for the ΔT = -80 K case, associated to the appearance of the physically relevant contact zone. The results obtained for the comparison between G and G_c are shown in Figure 6. The choice of the appropriate value of G_{1c} for each λ considered is based on the same criterion previously employed for the $\Delta T = 0\ K$ case. The results shown in Figure 6 predict an unstable growth from the initial debond until a position of the lower crack tip α within the range (194º-200º). The end of the unstable growth for

the original case was located at $\alpha \cong 206º$ [6]. In this range a new phase of the mechanism of damage may take place: the kinking of the crack towards the matrix.

5. INTERFACE CRACK KINKING

The prediction of kinking of the interface crack towards the matrix, once the period of unstable growth along the interface has finished, consists of two steps: the search for the preferential direction of the incipient crack in the matrix and the evaluation of the possibility of this change in the propagation of the crack.

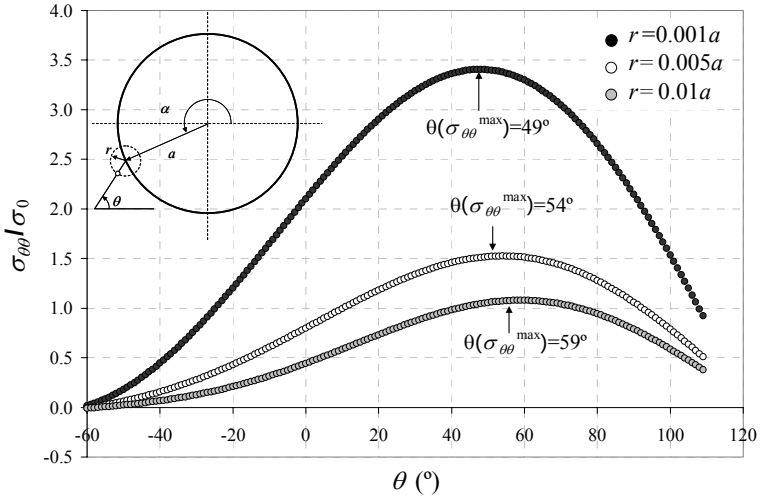

Figure 7. Circumferential stress state at the neighbourhood of $\alpha = 200º$ (ΔT = -80 K).

Referring to the first aspect, the application of the maximum circumferential stress criterion [16], at the neighbourhood of the interface crack tip within the α range of termination of unstable growth, allows the most favourable direction of the incipient crack in the matrix to be predicted. The application of this criterion for the $\Delta T = 0\ K$ case concluded that [7], if kinking took place it would occur for $\alpha \cong 206º$ in a direction within the range $\theta = 50º$-$58º$, with reference to the direction perpendicular to the applied load. The same analysis is presented in the present work for the ΔT = -80 K case, studying the circumferential stress state at the neighbourhood of the interface crack tip at the position $\alpha \cong 200º$ and for points located on three circumferences (radii $r = 0.001a$, $r = 0.005a$ and $r = 0.01a$) centred at the tip. The numerical results are shown in Figure 7 showing that the maximum circumferential stress is produced in a direction within the range $\theta = 49º$–$59º$. This range is very similar to that found for the $\Delta T = 0\ K$ case, is above 45º and includes the experimental macro-failure orientation angle, 53º.

It is in any case interesting to analyse the sensitivity of the plausible directions of kinking to the position of the lower crack tip. In this sense Figure 8 includes the results of the numerical model associated to the range of preferential kinking directions corresponding to different positions of the lower crack tip, together with the predictions carried out by means of the analytical solution by Comninou [17]. The results shown in the Figure present a low sensitivity to the position of the lower crack tip, specially once a physically relevant contact zone is developed. The predicted orientation range by the numerical model always maintains its lower boundary above 45º and shows an amplitude that narrows as the position of the lower crack tip moves forward, its mean value being around 53º.

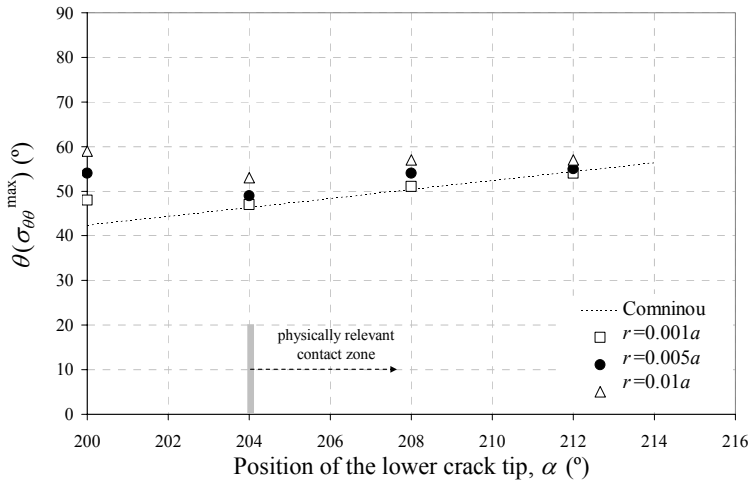

Figure 8 $\theta\left(\sigma_{\theta\theta}^{\max}\right)$ predictions versus α.

With reference to the energetic possibilities of kinking occurrence, the values of the energy release rate for an interface crack that has kinked into the matrix, G^m, from a position at the interface corresponding to $\alpha = 200º$ are calculated making use of the model shown in Figure 2b and plotted in Figure 9 for four different orientations of the kinked crack $\theta = 45º, 50º, 55º$ and $60º$. In this Figure the value of the energy release rate associated to the crack at the interface, G^{int}, for $\alpha = 200º$, is also included. The comparison between G^m and G^{int} shows that G^{int} is slightly greater than G^m for all orientations in the matrix considered. Taking into account that, although G_{IIc}^{int} values are usually greater than the G_{Ic}^m ones, which would support the kinking occurrence at $\alpha = 200º$, this tendency may not be maintained for all types of interfaces, and, therefore in those cases, no determining energetic arguments would exist for decide between kinking at $\alpha = 200º$ or further extension along the interface.

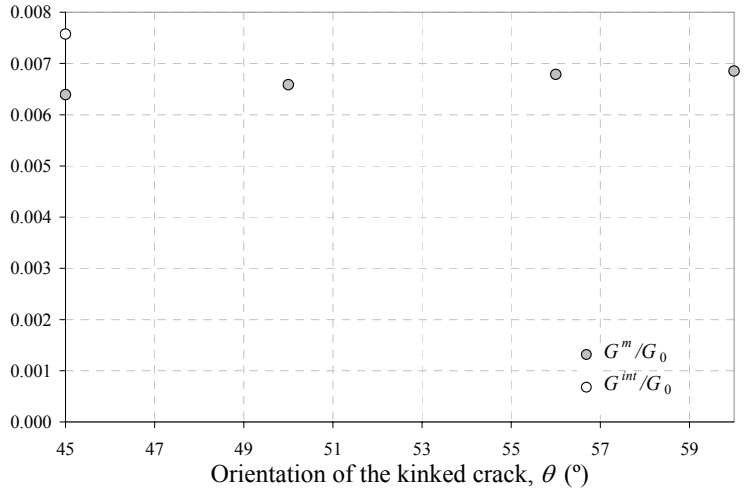

Figure 9. G^m and G^{int} versus α (ΔT = -80 K, $\alpha = 200º$).

At this point, remembering that the appearance of the contact zone at the lower crack tip was detected for positions a little bit higher than $\alpha = 200º$ (in fact $\alpha = 202º$), Figure 4, and the low sensitivity of the range of preferential orientations in the matrix to the lower crack tip position, Figure 8, it seems interesting to analyse the energetic

possibilities of kinking from an interface crack position where a physically relevant contact zone is already present, for instance $\alpha = 204º$. This analysis is included in Figure 10 where G_I^m, G_{II}^m and G^m for $\alpha = 204º$ are represented versus the orientation angle, as well as its associated value G^{int}. It can be seen in the Figure that Mode I clearly dominates the energy release rate values in the matrix, which are higher than G^{int} for all orientations considered. This result, combined with the assumption of similar values for G_{Ic}^m and G_{IIc}^m, would support the kinking of the interface crack towards the matrix. It can be also checked, using the adequate zoom, that, though the G^m values are similar for all orientations considered, the maximum, strictly speaking, is found for $\theta = 53º$.

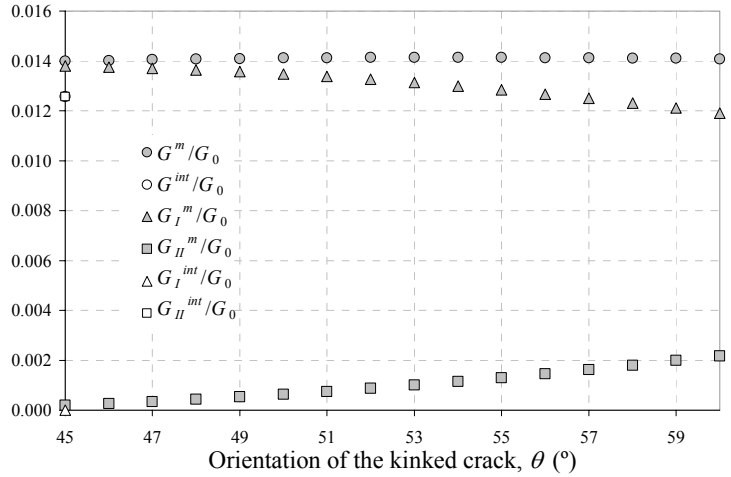

Figure 10. G^m and G^{int} versus θ (ΔT = -80 K, $\alpha = 204º$).

6. CONCLUSIONS

The effect of the presence of residual curing stresses on the mechanism of failure under compression has been analysed by means of a BEM model and making use of Interfacial Fracture Mechanics concepts.

The presence of residual curing stresses affects neither the appearance nor the initial growth of the first damage at the interface. Crack morphology is slightly altered since the consideration of curing stresses reduces the size of the 'bubble' at the lower crack tip and advances its closing. This fact influences the evolution of the energy release rate along the interface, mainly reducing the level of mode I component. All this lead to predictions of growth at the interface similar to that found without considering the presence of residual curing stresses, though an earlier end of the period of unstable growth at the interface is found. This result, together with the conclusions obtained from the kinking analysis, leads to a small advance of the position of kinking at the interface with reference to the results found when the residual curing stresses are not considered. In any case, the range of preferential kinking orientations detected is above 45º and includes the experimental macro-failure angle. Thus, the results shown in this work clarify the effect of residual curing stresses in the development of the inter-fibre failure at micromechanical level under compression, showing that there are no relevant differences with respect to the case in which these stresses are not considered. As a final remark, basic information for the development of a physically based failure criterion has been provided and, once more, the importance of micromechanics in the study of failure in composite materials is emphasized.

ACKNOWLEDGEMENTS

The work was supported by the Spanish Ministry of Education and Science (Projects TRA2005-06764 and TRA2006 08077) and Junta de Andalucía (Projects of Excellence TEP 1207 and TEP-02045).

REFERENCES

1- Andersson, B., Sjögren, A. and Berglund, L., "Micro- and meso-level residual stresses in glass-fiber/vinyl-ester composites", *Composites Science and Technology*: 2000;60: 2011-2028.
2- París, F., "A study of failure criteria of fibrous composite materials"; NASA/CR-2001-210661, 2001.
3- París, F., Correa, E. and Cañas, J., "Micromechanical view of failure of the matrix in fibrous composite materials", *Composites Science and Technology*: 2003;63:1041-1052.
4- París, F., Correa, E. and Mantič, V., "Kinking of transverse interface cracks between fibre and matrix" Journal of Applied Mechanics:2007;74(4):703-716.
5- Correa, E., Gamstedt, K.G., París, F. and Mantič, V. "Effect of the presence of compression in transverse cycling loading for fibre-matrix debonding of unidirectional composites plies", *Composites Part A: Applied Science and Manufacturing*: 2007;38:2260-2269.
6- Correa, E., Mantic, V. and París, F., "Numerical characterization of the fibre-matrix interface crack growth under transverse compression", Engineering Fracture Mechanics, doi:10.1016/j.engfracmech.2008.03.005.
7- Correa, E., Mantič, V. and París, F., "A micromechanical view of inter-fibre failure of composite materials under compression transverse to the fibres", *Composites Science and Technology*, doi:10.1016/j.compscitech.2008.02.022.
8- París, F. and Cañas, J., "Boundary Element Method. Fundamentals and Applications", 1997, Oxford, OUP.
9- Irwin, G.R., "Analysis of stresses and strain near the end of a crack transversing a plate", *Journal of Applied Mechanics*: 1957;24: 361-364.
10- Toya, M, "A crack along the interface of a circular inclusion embedded in an infinite solid", Journal of Mechanics and Physics of Solids:1974;22:325-348.
11- Murakami, Y., "Stress Intensity Factor Handbook",1988, Oxford, Pergamon Press.
12- Soden, P.D., Hinton, M.J. and Kaddour, A.S., "Lamina properties, lay-up configurations and loading conditions for a range of fibre-reinforced composite laminates", *Composites Science and Technology*:1998;58:1011-1022.
13- Mantič, V., Blázquez, A., Correa, E. and París, F., "Analysis of interface cracks with contact in composites by 2D BEM", Guagliano, M. and Aliabadi, M.H. eds. Fracture and Damage of Composites, WIT Press, UK, 2006:189-241.
14- Hutchinson, J.W. and Suo, Z., "Mixed mode cracking in layered materials", *Advances in Applied Mechanics*:1992;29:63-191.
15- Mantič, V. and París, F., "Relation between SIF and ERR based measures of fracture mode mixity in interface cracks", *International Journal of Fracture*: 2004;130:557-569.
16- Erdogan, F. and Sih, G.C, "On the crack extension in plates under plane loading and transverse shear", *Journal of Basic Engineering*: 1963;85:519-527.
17- Comninou, M., "The interface crack", Journal of Applied Mechanics: 1977;44:631-636.